

# Short-baseline electron antineutrino disappearance study by using neutrino sources from $^{13}\text{C} + ^9\text{Be}$ reaction

Jae Won Shin,<sup>a</sup> Myung-Ki Cheoun,<sup>a,1</sup> Toshitaka Kajino<sup>b,c</sup> and Takehito Hayakawa<sup>d</sup>

<sup>a</sup>Department of Physics and Origin of Matter and Galaxy Evolution (OMEG) Institute, Soongsil University, Seoul 156-743, Korea

<sup>b</sup>Division of Theoretical Astronomy, National Astronomical Observatory of Japan, Mitaka, Tokyo 181-8588, Japan

<sup>c</sup>Department of Astronomy, Graduate School of Science, University of Tokyo, Hongo, Bunkyo-ku, Tokyo 113-0033, Japan

<sup>d</sup>Quantum Beam Science Directorate (QUBS), Japan Atomic Energy Agency (JAEA), 2-4 Shirane, Shirakata, Tokai-mura, Naka-gun, Ibaraki 319-1195, Japan

E-mail: [shine8199@skku.edu](mailto:shine8199@skku.edu), [cheoun@ssu.ac.kr](mailto:cheoun@ssu.ac.kr), [kajino@nao.ac.jp](mailto:kajino@nao.ac.jp), [hayakawa.takehito@qst.go.jp](mailto:hayakawa.takehito@qst.go.jp)

**Abstract.** To investigate the existence of sterile neutrino, we propose a new neutrino production method using  $^{13}\text{C}$  beams and a  $^9\text{Be}$  target for short-baseline electron antineutrino ( $\bar{\nu}_e$ ) disappearance study. The production of secondary unstable isotopes which can emit neutrinos from the  $^{13}\text{C} + ^9\text{Be}$  reaction is calculated with three different nucleus-nucleus (AA) reaction models. Different isotope yields are obtained using these models, but the results of the neutrino flux are found to have unanimous similarities. This feature gives an opportunity to study neutrino oscillation through shape analysis. In this work, expected neutrino flux and event rates are discussed in detail through intensive simulation of the light ion collision reaction and the neutrino flux from the beta decay of unstable isotopes followed by this collision. Together with the reactor and accelerator anomalies, the present proposed  $\bar{\nu}_e$  source is shown to be a practically alternative test of the existence of the  $\Delta m^2 \sim 1 \text{ eV}^2$  scale sterile neutrino.

**Keywords:** Short baseline neutrino disappearance, Electron antineutrino source, Sterile neutrinos, Nucleus-nucleus collision

---

<sup>1</sup>Corresponding author.

---

## Contents

<b>1</b>	<b>Introduction</b>	<b>1</b>
<b>2</b>	<b>Methods</b>	<b>2</b>
2.1	Proposed experimental setup	2
2.2	Electron antineutrino detection	3
2.3	Simulation tool and nucleus-nucleus reaction models	3
<b>3</b>	<b>Results</b>	<b>5</b>
3.1	Production isotope yields in $^9\text{Be}$ target	5
3.2	Neutrino energy spectra from $^9\text{Be}$ target	6
3.3	Electron antineutrinos produced in the neutrino production targetry	8
<b>4</b>	<b>Short-baseline electron antineutrino disappearance studies and sterile neutrino</b>	<b>9</b>
<b>5</b>	<b>Summary and Conclusion</b>	<b>11</b>

---

## 1 Introduction

Over the past few decades, a considerable number of studies has been done on the neutrino oscillation with a great success of measuring neutrino mixing angles. However, some experiments for the neutrino oscillation revealed more or less disagreements with the three-flavor neutrino model, which termed as neutrino anomalies, as reported in LSND [1], MiniBoone [2], reactor experiments [3] and gallium experiments [4]. One of the approaches for explaining the neutrino anomalies is to presume the existence of the hypothetical fourth neutrino, which is called as sterile neutrino, because the sterile neutrino does not interact with other particles except for a mixing with active neutrinos.

The possibility of the existence of sterile neutrino triggered by the lots of anomalies is now being widely discussed in the filed of particle, nuclear physics, and astrophysics including cosmology. Most of the neutrino experiments are classified into the long-base line accelerator and the short-base line reactor neutrino experiments. The former neutrino source comes from high-energy proton accelerators; this source produces high-energy and high-flux neutrinos from the pion or kaon decay at rest or in flight and utilize long-distance detectors from the accelerator except for the MiniBooNE-like experiments. On the contrary, the latter one relies on neutrinos from nuclear reactors, which enables to use relatively the short-distance detector from the source, but needs to pin down the ambiguity on the neutrino spectrum stemming from vast numbers of nuclear fissions in the reactor [5]. Here, it should be noted that recent results from the IceCube neutrino telescope, which limits on the mixing of sterile neutrino and muon neutrino, does not constrain the neutrino mixing angle relevant to the reactor anomaly [6].

Recently many interesting studies for the existence of sterile neutrinos ( $\nu_s$ ) are proposed with antineutrino sources from radioactive isotopes or an accelerator-based Isotope Decay-At-Rest (IsoDAR) concept [7–11]. They utilize different neutrino sources from the two neutrino sources mentioned above. For instance, KamLAND (CeLAND) [8] and Borexino (Short

distance neutrino Oscillations with BoreXino (SOX)) [9] plan to perform experiments using approximately 100 kCi of  $^{144}\text{Ce}$ - $^{144}\text{Pr}$  radio isotopes which can generate antineutrinos with energy of up to 3 MeV. As another type source, electron antineutrinos ( $\bar{\nu}_e$ ) produced by  $^8\text{Li}$  using an accelerator-based IsoDAR concept was proposed [10, 12]. The  $\bar{\nu}_e$  from  $^8\text{Li}$  has higher energy than that from  $^{144}\text{Ce}$ - $^{144}\text{Pr}$ , and thus can be used for study of antineutrino spectrum distortion in the energy region of  $5 \text{ MeV} < E_{\bar{\nu}} < 7 \text{ MeV}$ , where some distortions or anomalies are reported by the reactor antineutrino experiments (Daya Bay [13], Double Chooz [14] and RENO [15, 16]).

On the other hand, there are many ion beam facilities such as FAIR at GSI, FRIB at MSU, HRIBF at ORNL, ISAC at TRIUMF, ISOLDE at CERN, RIBF at RIKEN, SPES at INFN, and SPIRAL2 at GANIL. They have been designed or are being developed to obtain features (e.g. use of high-intensity high-power primary beams, use of large-aperture high-field superconducting magnets, etc.) suitable for variety scientific purposes [17–20]. The ion beams can provide us with new opportunities in neutrino physics, especially, for production of artificial neutrino sources. By using the ion beams with compact neutrino detectors such as DANSS [21], NEUTRINO4 [22], NUCIFER [23], PANDA [24], PROSPECT [25], and STEREO [26] which have been planned to measure reactor neutrinos at a distance of several meters, we can test the existence of sterile neutrinos, in particular, on 1 eV mass scale.

In this work, to study the possibility of sterile neutrino, we propose a new neutrino production method with a  $^{13}\text{C}$  beam and a  $^9\text{Be}$  target. Unstable isotopes such as  $^8\text{Li}$  and  $^{12}\text{B}$  can be produced through the  $^{13}\text{C} + ^9\text{Be}$  reaction and decay subsequently. Thus, we can obtain new neutrino sources ( $\bar{\nu}_{^{13}\text{C}+^9\text{Be}}$ ) from the possible beta decay processes of unstable isotopes produced at the  $^{13}\text{C} + ^9\text{Be}$  reaction. In a sense, the production mechanism is similar to that of reactor neutrinos. However, in this case, neutrino energy spectrum is much easier identified compared with those of reactor neutrinos because the number of isotopes is limited and the geometry is simple. The production of secondary isotopes from the  $^{13}\text{C} + ^9\text{Be}$  reaction is calculated using the GEANT4 particle transport Monte Carlo code [27, 28], with three different nucleus-nucleus (AA) reaction models. Different isotope yields are obtained using these models, but the results of the neutrino flux are shown to have a striking similarity. This unique feature gives a chance to neutrino oscillation study through shape analysis regardless of the theoretical AA models considered. Expected neutrino flux and event rates including the sterile neutrino contribution are discussed in this work.

Outline of the paper is as follows. In section 2, proposed experimental setup, the neutrino detection and simulation tools including the nuclear reaction model are described. In section 3, the results of expected neutrino flux and event rates are presented, and neutrino disappearance features and possible reaction rate changes by the sterile neutrino are discussed with possible inherent errors in section 4. A summary is given in section 5.

## 2 Methods

### 2.1 Proposed experimental setup

We propose an electron antineutrino source using an accelerator-based IsoDAR concept with a  $^{13}\text{C}$  beam and a  $^9\text{Be}$  target. 75 MeV/u  $^{13}\text{C}$  beam with a current of 300  $\mu\text{A}$ , namely 293 kW of beam power, is considered in this work. There are many ion beam facilities which have been designed and are being developed with advanced features (e.g. use of high-intensity high-power primary beams). For example, a beam power of 400 kW is aimed to achieve at FRIB (MSU). In this regard, the present proposal is a feasible experimental plan.

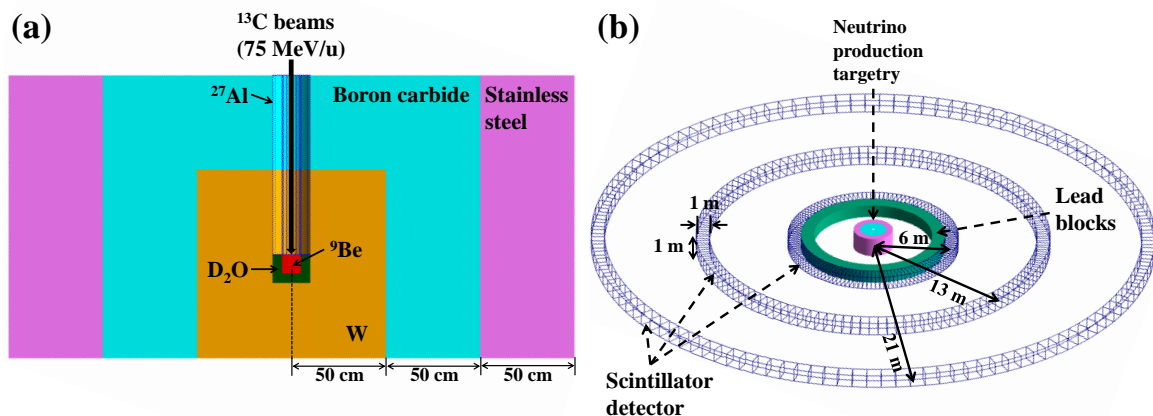


**Figure 1.** (Color online) (a) A schematic cross section view showing neutrino production targetry. (b) A schematic view showing proposed short baseline experiment setup.

Figure 1 (a) shows geometrical setups for the neutrino production. The  ${}^9\text{Be}$  target is modeled as a cylinder of a radius of 5 cm and a thickness of 10 cm. Neutrinos are obtained from unstable isotopes produced through the  ${}^{13}\text{C} + {}^9\text{Be}$  reaction. The  ${}^9\text{Be}$  target is surrounded by a  $\text{D}_2\text{O}$  layer with 5 cm thickness for cooling. In addition, tungsten, boron carbide, and stainless steel layers surround the  ${}^9\text{Be}$  target and the  $\text{D}_2\text{O}$  layer for effective secondary neutron generation and shielding of  $\gamma$ -rays.

The electron antineutrino source proposed in this work can be useful for the neutrino disappearance study of the investigation of the existence of fourth neutrino, sterile neutrino. Figure 1 (b) shows the proposed short-baseline experiment setup consisting of the neutrino production targetry and the detection sector. Lead blocks with 1 m thickness surround the neutrino production targetry to shield the radiation from the targetry. In this work, we consider three ring-shape detectors with a height of 1 m and a thickness of 1 m.

## 2.2 Electron antineutrino detection

For electron antineutrino detection, an inverse beta decay (IBD) reaction,  $\bar{\nu}_e + p \rightarrow e^+ + n$ , is considered in this work. This IBD reaction in neutrino detection offers two signals : a prompt signal due to the annihilation of a positron and a delayed signal of 2.2 MeV  $\gamma$ -ray following neutron capture. Characteristics of two distinct detections can make efficient rejection of possible backgrounds. The energy dependent cross section of the IBD reactions can be expressed by [29]

$$\sigma_{\bar{\nu}_e}(E_{\bar{\nu}_e}) \approx p_e E_e E_{\bar{\nu}_e}^{-0.07056+0.02018\ln E_{\bar{\nu}_e}-0.001953\ln^3 E_{\bar{\nu}_e}} \times 10^{-43} [\text{cm}^2], \quad (2.1)$$

where  $p_e$ ,  $E_e$ , and  $E_{\bar{\nu}_e}$  are the positron momentum, the total energy of the positron, and the energy of  $\bar{\nu}_e$  in MeV, respectively. Note that the mass difference between  $m_n$  and  $m_p$  can be described as  $E_e = E_{\bar{\nu}_e} - \Delta$ , where  $\Delta = m_n - m_p \approx 1.293$  MeV. This cross section agrees within few per-mille with the fully calculated results including the radiative corrections and the final-state interactions in IBD.

## 2.3 Simulation tool and nucleus-nucleus reaction models

We have performed GEANT4 [27, 28] simulations for estimating the production yields of isotopes by considering the bombardment of 75 MeV/u  ${}^{13}\text{C}$  beams on the  ${}^9\text{Be}$  target as

shown in figure 1. In these calculations, we use the `G4ComponentGGNuclNuclXsc` class for the calculation of overall cross sections of AA reactions and the `G4ionIonisation` class for ionization processes. The `G4ComponentGGNuclNuclXsc` class provides total, inelastic, and elastic cross sections for the AA reactions using the Glauber model with Gribov corrections [30–33] where this class is valid for all incident energies above 100 keV. The `G4ionIonisation` class is used for the calculation of the ionization processes, where the effective charge approach [34] and the ICRU 73 [35] table for the stopping power are used.

An important point in the calculation of heavy ion collision reactions is the choice of hadronic models. To discuss the relative isotope production yields caused by different AA reactions, three different hadronic models; `G4BinaryLightIonReaction` [36, 37], `G4QMDReaction` [38] and `G4INCLXXInterface` [39, 40] are used. They are described in detail in the Physics Reference Manual [41] on the web [42]. Here, we list some key features of them for the readers’ convenience. We distinguish our model calculations by referring to `G4BinaryLightIonReaction`, `G4INCLXXInterface`, and `G4QMDReaction` simply as “G4BIC”, “G4INCL” and “G4QMD”, respectively.

**G4BIC** : The `G4BinaryLightIonReaction` class is an extension of `G4BinaryCascade` for light ion reactions. It is a data driven from the Intra-Nuclear Cascade model based on a detailed 3-D model of the nucleus and binary scattering between reaction participants and nucleons within the nuclear model. Participant particles are either a primary particle including nucleons in a projectile nucleus, or particles generated or scattered in the process of cascade. Each participating particle is seen as a Gaussian wave packet and total wave function is assumed to be a direct product of the wave functions of the participating particles without antisymmetrization. The equations of motion has the same structure as the classical Hamilton equations, where the Hamiltonian is calculated from a simple time-independent optical potential. The nucleon distribution follows a Woods-Saxon model for heavy nuclei ( $A > 16$ ) and a harmonic-oscillator shell model for light nuclei ( $A < 17$ ). Participant particles are only propagated in the nucleus, and participant-participant interactions are not taken into account in the model. The cascade terminates when mean kinetic energy of scattered particles (participants within the nucleus) has dropped below a threshold (15 MeV). After the cascade termination, properties of the residual excitation system and the final nuclei are evaluated. Then, the residual participants and the nucleus in that state are treated by pre-equilibrium decay. For statistical description of particle emission from excited nuclei, the `G4ExcitationHandler` class is used. For light ion reactions, projectile excitations are determined from the binary collision participants using the statistical approach towards excitation energy calculation in an adiabatic abrasion process. Given this excitation energy, the projectile fragment is then treated by the `G4ExcitationHandler`.

**G4QMD** : `G4QMDReaction` is based on a quantum extension of the classical molecular dynamics (QMD). It is widely used to simulate AA reactions for many-body processes, in particular, the formation of complex fragments. QMD has similar characteristics to Binary Cascade in treating each participant particle as a Gaussian wave packet and assuming total wave function to the direct product of the participants. Comparing with Binary Cascade, however, QMD has some different characteristics such as the definition of a participant particle, potential term in the Hamiltonian and participant-participant interactions. Participant particles in the QMD mean entire nucleons in the target and projectile nucleus. The potential terms of the Hamiltonian in QMD are calculated from the entire relation of particles in the system where the potential includes a Skyrme type interaction, a Coulomb interaction and a symmetry term. Because there is no criterion between participant particle and

others in QMD, participant-participant interactions are naturally included. There are many different types of QMD models, but G4QMDReaction is based on JAERI Quantum Molecular Dynamics (JQMD) [43]. The self-generating potential field is used in G4QMD, and the potential field and the field parameters of G4QMD are also based on JQMD with Lorentz scalar modifications. In the G4QMDReaction, the reaction processes are also described by two steps. First, as a dynamical process, the direct reactions, non-equilibrium reactions, and dynamical formation of highly excited fragments are calculated in the manner of QMD. Second, as a statistical process, evaporation and fission decays are performed for the excited nucleons produced in the first step. As the excitation model, GEM (generalized evaporation model) [44] is used.

**G4INCL** : This class is being used for reactions induced by nucleons, pions and light ion on any nucleus using the INCL++ model, which is a version of Liège intranuclear-cascade model (INCL) [45] fully re-written in C++. For light ion induced reactions, the projectile is described as a collection of independent nucleons with gaussian momentum and position distributions which use the realistic standard deviation of the projectile ion for the position distribution. Momenta and positions of the nucleons inside a target nucleus are determined by modeling the nucleus as a free Fermi gas in a static potential well with a realistic density. The reaction is described as an avalanche of binary nucleon-nucleon collisions, which can lead to the emission of energetic particles and to the formation of an excited thermalised nucleus as remnant. Particles in the model are labeled either as participants (projectile particles and particles that have undergone a collision with a projectile) or spectators (target particles that have not undergone any collision). Collisions between spectator particles are neglected. The projectile (light ion) follows globally a classical Coulomb trajectory until one of its nucleon impinges on a spherical calculation volume around the target nucleus, which is large enough to marginally neglect nuclear interactions. The nucleons entering the calculation sphere move globally (with the beam velocity) until one of them interacts with a target nucleon. The nucleon-nucleon (NN) interaction is then computed with the individual momenta with Pauli blocking restriction. Nucleons crossing the sphere of the calculation without any NN interactions are also combined in the “projectile spectator” at the end of the cascade. The cascade stops when the remnant nucleus shows signs of thermalization; a rather unique aspect of INCL is the self-consistent determination of the cascade stopping time. The projectile spectator nucleus is kinematically defined by its nucleon content and its excitation energy obtained by an empirical particle-hole model, and then the de-excitation of the projectile fragments is described by the G4ExcitationHandler class.

Many different isotopes produced via the  $^{13}\text{C} + ^9\text{Be}$  reaction can emit neutrinos with various energies. The energy distributions of the neutrinos are calculated using “G4RadioactiveDecay” [46, 47] class based on the Evaluated Nuclear Structure Data File (ENSDF) [48].

## 3 Results

### 3.1 Production isotope yields in $^9\text{Be}$ target

The numbers of unstable isotopes accumulated inside the  $^9\text{Be}$  target, obtained using G4BIC, G4INCL, and G4QMD, are plotted in figure 2 (a). The figure shows that electron antineutrinos via the 75 MeV/u  $^{13}\text{C} + ^9\text{Be}$  reaction are generated through  $\beta$  decay from  $^6\text{He}$ ,  $^8\text{Li}$ ,  $^9\text{Li}$ ,  $^{12}\text{Be}$ ,  $^{12}\text{B}$ , and  $^{13}\text{B}$ , where the summation of their fractions are 99%, 96%, and 97.0% for G4BIC, G4INCL, and G4QMD, respectively. Because the half-lives of those isotopes are

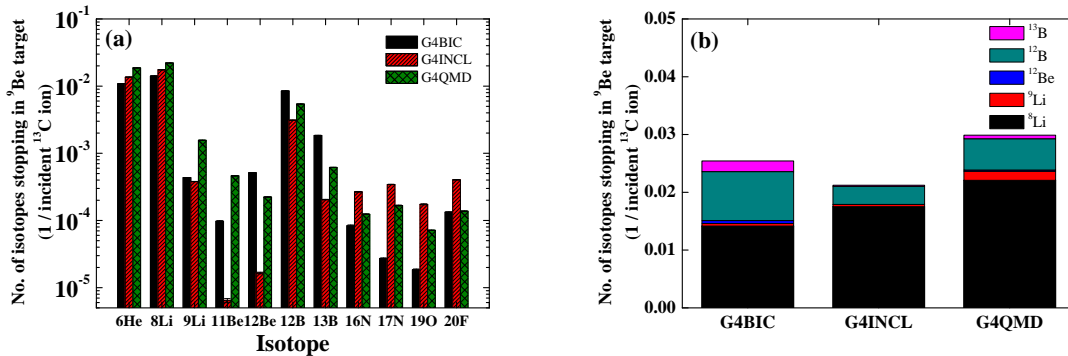


**Figure 2.** (Color online) Production isotope yields (a) and their sums (b) in  ${}^9\text{Be}$  target obtained from G4BIC, G4INCL, and G4QMD.  ${}^6\text{He}$  is not shown in (b) because the neutrino energy from  ${}^6\text{He}$  is lower than the detection threshold energy of 4 MeV.

**Table 1.** Radioactive decay data for the isotopes produced in  ${}^9\text{Be}$  target.

Isotope	half-life [sec.]	decay mode	Branching ratio [%]	$Q$ Value [MeV]
${}^6\text{He}$	0.8067	${}^6\text{He} \rightarrow e^- + \bar{\nu}_e + {}^6\text{Li}$	100	3.5078
${}^8\text{Li}$	0.838	${}^8\text{Li} \rightarrow e^- + \bar{\nu}_e + {}^8\text{Be}$	100	16.097
${}^9\text{Li}$	0.1783	${}^9\text{Li} \rightarrow e^- + \bar{\nu}_e + {}^9\text{Be}$	50.5	13.606
	0.1783	${}^9\text{Li} \rightarrow e^- + \bar{\nu}_e + n + {}^8\text{Be}$	49.5	11.941
${}^{12}\text{Be}$	0.0213	${}^{12}\text{Be} \rightarrow e^- + \bar{\nu}_e + {}^{12}\text{B}$	100	11.708
${}^{12}\text{B}$	0.0202	${}^{12}\text{B} \rightarrow e^- + \bar{\nu}_e + {}^{12}\text{C}$	100	13.3689
${}^{13}\text{B}$	0.01736	${}^{13}\text{B} \rightarrow e^- + \bar{\nu}_e + {}^{13}\text{C}$	100	13.4372

shorter than a few seconds, the electron antineutrinos are predominantly produced from the  ${}^9\text{Be}$  target during the  ${}^{13}\text{C}$  beam irradiation.

The isotopes except for  ${}^6\text{He}$  emit electron antineutrinos which have a maximum flux in the energy range of  $6 \text{ MeV} < E_{\bar{\nu}_e} < 7 \text{ MeV}$  as shown in figure 3, and their fractions are shown in figure 2 (b). Besides low energy neutrinos from  ${}^6\text{He}$ , dominant contribution comes from  ${}^8\text{Li}$  and sub-dominant contribution is  ${}^{12}\text{B}$ . The summation of their fractions calculated using G4BIC, G4INCL, and G4QMD are 0.025, 0.021, and 0.03 per incident  ${}^{13}\text{C}$  ion, respectively. This result indicates very similar shape of neutrino spectra regardless of the AA reaction model considered in this work. In the  ${}^9\text{Be}$  target,  ${}^{10}\text{Be}$  and  ${}^{14}\text{C}$  are produced in addition to the isotopes in figure 2 (a). Due to very long half-lives of  ${}^{10}\text{Be}$  ( $1.5 \times 10^6 \text{ y}$ ) and  ${}^{14}\text{C}$  ( $5.7 \times 10^3 \text{ y}$ ), their contributions for neutrino production are marginal, and thus they are neglected in this work.

### 3.2 Neutrino energy spectra from ${}^9\text{Be}$ target

To see expected energy spectrum of all electron antineutrino from the  ${}^9\text{Be}$  target, we first obtain the energy spectra from main isotopes such as  ${}^6\text{He}$ ,  ${}^8\text{Li}$ ,  ${}^9\text{Li}$ ,  ${}^{12}\text{Be}$ ,  ${}^{12}\text{B}$ , and  ${}^{13}\text{B}$ . Radioactive decay data of these isotopes are tabulated in Table 1, and their neutrino energy distributions are plotted in figure 3. The spectrum of the electron antineutrinos from  ${}^6\text{He}$

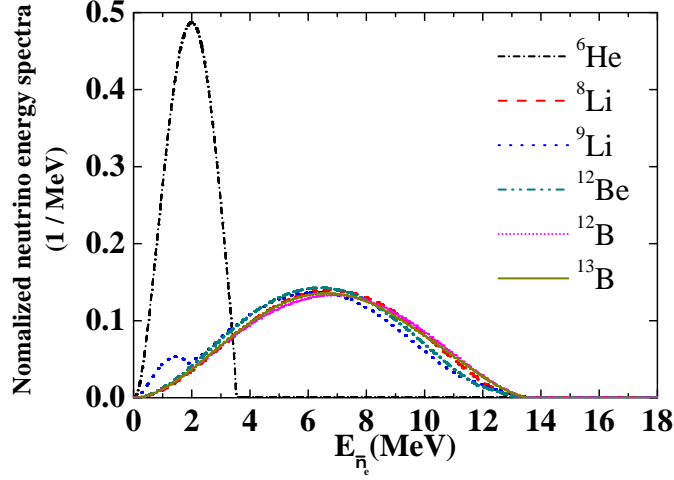


**Figure 3.** (Color online) Expected neutrino energy distributions from  ${}^6\text{He}$ ,  ${}^8\text{Li}$ ,  ${}^9\text{Li}$ ,  ${}^{12}\text{Be}$ ,  ${}^{12}\text{B}$ , and  ${}^{13}\text{B}$  isotopes. Decays of  $10^9$  for each isotope are simulated, but all presented results except for  ${}^{12}\text{Be}$  are divided by  $10^9$ . For  ${}^{12}\text{Be}$ , the results are divided by  $2 \times 10^9$  because  ${}^{12}\text{B}$  which is the daughter nucleus of  ${}^{12}\text{Be}$  also emits neutrinos.

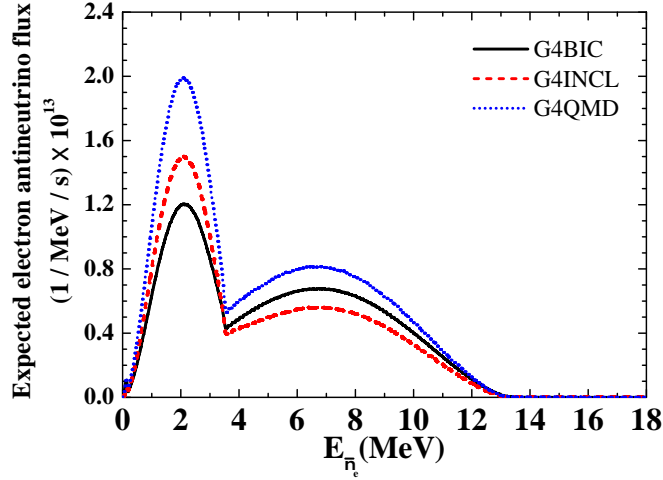


**Figure 4.** (Color online) Expected electron antineutrino flux in  ${}^9\text{Be}$  target where the neutrinos are produced by  $75 \text{ MeV/u } {}^{13}\text{C} + {}^9\text{Be}$  reaction. The solid line, the dashed line, and the dotted line are denote the results obtained from G4BIC, G4INCL, and G4QMD, respectively. The  $300 \mu\text{A}$  current is assumed.

have a peak at  $E_{\bar{\nu}_e} = 2 \text{ MeV}$  and a width of  $3.5 \text{ MeV}$ . The other spectra have similar distributions.

Expected electron antineutrino spectra for the  ${}^9\text{Be}$  target due to the  ${}^{13}\text{C} + {}^9\text{Be}$  reaction are plotted in figure 4, where  $75 \text{ MeV/u } {}^{13}\text{C}$  beams with  $300 \mu\text{A}$  current are assumed. Two



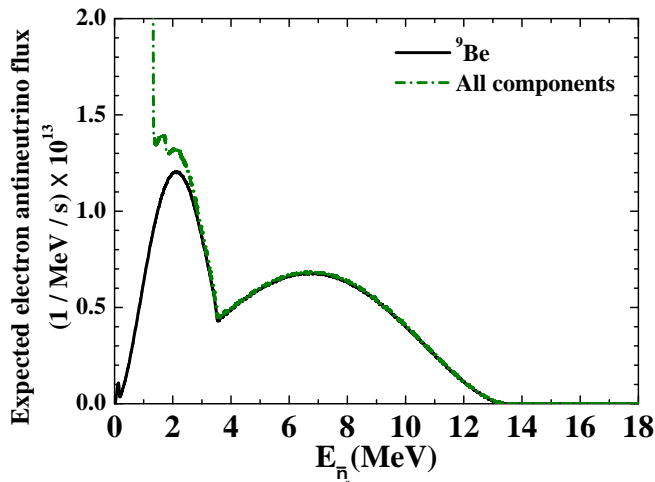


**Figure 5.** (Color online) Expected electron antineutrino flux produced in the  ${}^9\text{Be}$  target and the summation of all components in figure 1.

distinct broad peaks around  $E_{\bar{\nu}_e} = 2$  MeV and 7 MeV are shown in the figure 4 regardless of the nuclear reaction model predictions. The lower energy peak predominantly come from  ${}^6\text{He}$  and the higher energy peak originates from  ${}^8\text{Li}$ ,  ${}^9\text{Li}$ ,  ${}^{12}\text{Be}$ ,  ${}^{12}\text{B}$ , and  ${}^{13}\text{B}$ , as shown in figure 3. It should be noted that the spectral shapes in the energy region of  $E_{\bar{\nu}_e} > 4$  MeV turn out to be almost identical by multiplying the flux from G4BIC, G4INCL, and G4QMD by 1.2, 1.46, and 1, respectively. This characteristic enables us to perform model-independent shape analysis.

### 3.3 Electron antineutrinos produced in the neutrino production targetry

Electron antineutrinos can be practically produced in all components of the production targetry around the  ${}^9\text{Be}$  target in figure 1. Figure 5 show the calculated results where the dotted line and the solid line mean summations of the all components and the only  ${}^9\text{Be}$  target in figure 1, respectively. For decay modes, we consider fully the decays of the isotopes with half-life shorter than 10 yr. Because all of the results from the three different reaction models mentioned in section 2 provide the similar spectra, we only plot the result using G4BIC in figure 5.

The contribution of the neutrino from the  ${}^9\text{Be}$  target is dominant in the energy region of  $E_{\bar{\nu}_e} > 3$  MeV, but the other components are dominant for  $E_{\bar{\nu}_e} < 1$  MeV. Especially, in the energy region of  $E_{\bar{\nu}_e} > 4$  MeV, the contribution from the  ${}^9\text{Be}$  target is 99% of the total neutrinos. If we consider the neutrino energy cut of  $E_{\bar{\nu}_e} = 4$  MeV for electron antineutrino detection, we can effectively remove background neutrino signals from the other components. It means that the neutrino source can be concentrated on a small volume of the  ${}^9\text{Be}$  target. This feature can provide point like source experiments.

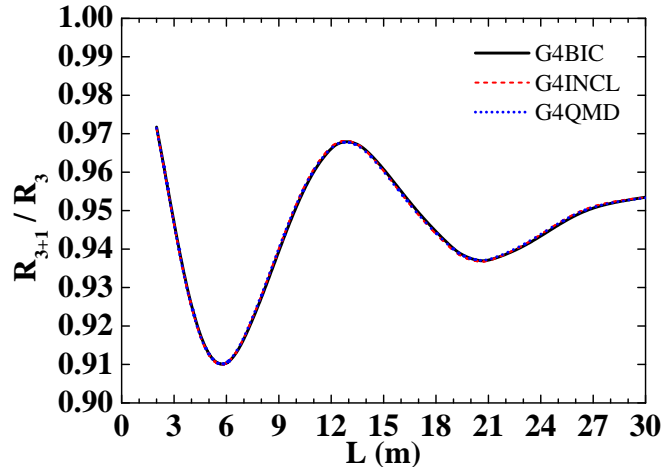


**Figure 6.** (Color online) Expected event rates with  $P_{3+1}$  model to those with  $P_3$  model ratios with respect to  $L$  are plotted.  $L$  is the distance between the neutrino source and the center of the scintillator detector.

#### 4 Short-baseline electron antineutrino disappearance studies and sterile neutrino

To check the existence of the fourth neutrino, we compare the event rates under electron antineutrino survival probabilities in the standard 3-flavor neutrino model ( $P_3$ ) and the 3+1 model ( $P_{3+1}$ ). For the calculation of  $P_3$ , we use the equation given by [49]

$$P_3 = 1 - \sin^2 2\theta_{13} S_{23} - c_{13}^4 \sin^2 2\theta_{12} S_{12}, \quad (4.1)$$

where  $S_{23} = \sin^2(\Delta m_{32}^2 L/4E)$  and  $S_{12} = \sin^2(\Delta m_{21}^2 L/4E)$ .  $L$  and  $E$  mean the source to detector distance and the neutrino energy, respectively. The neutrino oscillation parameters in Eq. (4.1) are taken from a global fit [50]. Electron-antineutrino survival probabilities in the 3+1 model can be written as

$$P_{3+1} = 1 - 4|U_{e4}|^2(1 - |U_{e4}|^2)\sin^2\left(\frac{\Delta m_{41}^2 L}{4E}\right). \quad (4.2)$$

The oscillation parameters in Eq. (4.2) are taken from the best-fit points by the 3+1 model for the combined short base lines (SBL) and IceCube data sets [51].

Ratios of the expected total event rate for the  $P_{3+1}$  model to that for the  $P_3$  model ( $R_{3+1\text{-to-}R_3}$ ) are calculated using the G4BIC, G4INCL, and G4QMD models (see figure 6). Here we assume the neutrino cut-off energy of 4 MeV. Even for the case without the energy cut, we obtained almost same results compared to those from calculations with the cut. All of the results using the three models are almost unanimous regardless of  $L$ . The  $R_{3+1\text{-to-}R_3}$  ratios show oscillation, and the minimum and the maximum values of the  $R_{3+1\text{-to-}R_3}$  are 0.91 at  $L = 6$  m and 0.97 at  $L = 13$  m, respectively. If there are no sterile neutrinos, the ratio should be 1.

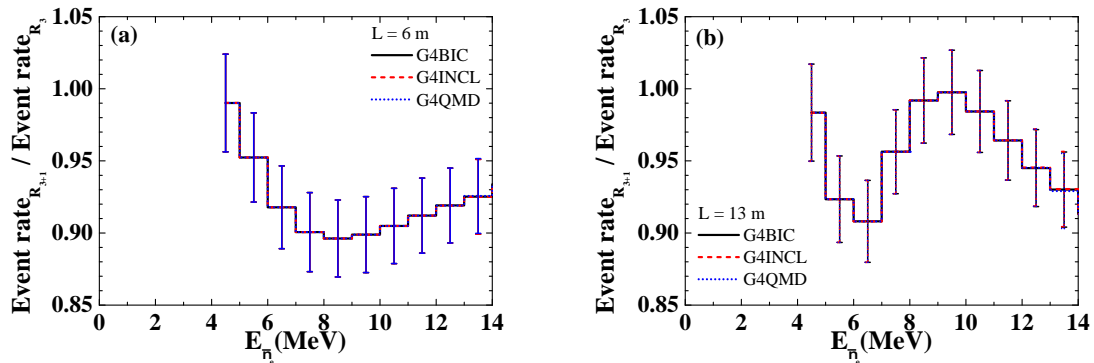


**Figure 7.** (Color online) Ratios of  $R_{3+1}$ -to- $R_3$  with respect to  $E_{\bar{\nu}_e}$  at (a)  $L = 6$  m and (b)  $L = 13$  m are shown.

Spectral shapes of the measured neutrinos would also give a chance to study the existence of fourth neutrinos.<sup>1</sup> To see the effect of possible sterile neutrinos using the shape analysis like Daya Bay [13], Double Chooz [14], and RENO [15, 16] experiments, the event rates are calculated for different  $L$  values using the ring detectors as shown in figure 1 (b). For the reconstruction of  $\bar{\nu}_e$  energy spectra, a liquid scintillator detector based on PROSPECT type detector [25] is considered. In the present oscillation analysis, we assumed an statistical error of 1.5%, a systematic error of 2%, an energy resolution of  $4.5\%/\sqrt{E/\text{MeV}}$ , a position resolution of 15 cm, and a IBD cross section error of 0.5% [25]. We use the cross section obtained using Eq. (2.1).

The  $R_{3+1}$ -to- $R_3$  ratios at  $L = 6$  m and  $L = 13$  m are plotted in figure 7. It should be also noted that the results in figure 7 are almost identical independently of the hadronic models used in this work. In the energy region of  $4 \text{ MeV} < E_{\bar{\nu}_e} < 9 \text{ MeV}$  corresponding to the region of  $3 \text{ MeV} < E_{vis} < 8 \text{ MeV}$ , the  $R_{3+1}/R_3$  ratio at  $L = 6$  m rapidly decreases up to 0.9 as  $E_{\bar{\nu}_e}$  increases. At the energies of  $E_{\bar{\nu}_e} > 9 \text{ MeV}$ , however, the ratio increases as  $E_{\bar{\nu}_e}$  increases. The comparison of the results in figures 7 (a) and (b) in the energy region of  $5 \text{ MeV} < E_{\bar{\nu}_e}$  can give a meaningful signal for the existence of hypothetical neutrinos. These characteristics are unique features of the present work due to the compact  $\bar{\nu}_e$  source.

Also, the comparison among the event rates for different  $L$  (e.g. near and far detectors of reactor neutrino experiments) can also be possible in this work. The ratios of the event rate at  $L = 13$  m to that at  $L = 21$  m with the  $P_{3+1}$  model are plotted in figure 8 (a). In the figure, the maximum and the minimum values are 1.11 at  $E_{\bar{\nu}_e} = 9.5 \text{ MeV}$  and 0.94 at  $E_{\bar{\nu}_e} = 13.5 \text{ MeV}$ , respectively. If we can measure approximately 17% deviation from the expected events, we can find a clue to the problem of whether the  $P_{3+1}$  model is the most appropriate scenario. Figure 8 (b) shows the results for  $R_{L=21m}/R_{L=6m}$ , which gives a different feature compared to that from figure 8 (a). The shapes in figures 8(a) and 8(b) can give effective chances to search for the existence of  $\nu_s$  and to test the 3+1 sterile neutrino scenario.

<sup>1</sup>The visible energy ( $E_{vis}$ ) of the prompt signal due to a positron ( $e^+$ ) is strongly correlated with the energy of  $\bar{\nu}_e$  ( $E_{\bar{\nu}_e}$ ),  $E_{\bar{\nu}_e} \simeq E_{vis} + 0.78 \text{ MeV}$ , which means that  $\bar{\nu}_e$  energy spectra can be reconstructed using the  $E_{vis}$ .

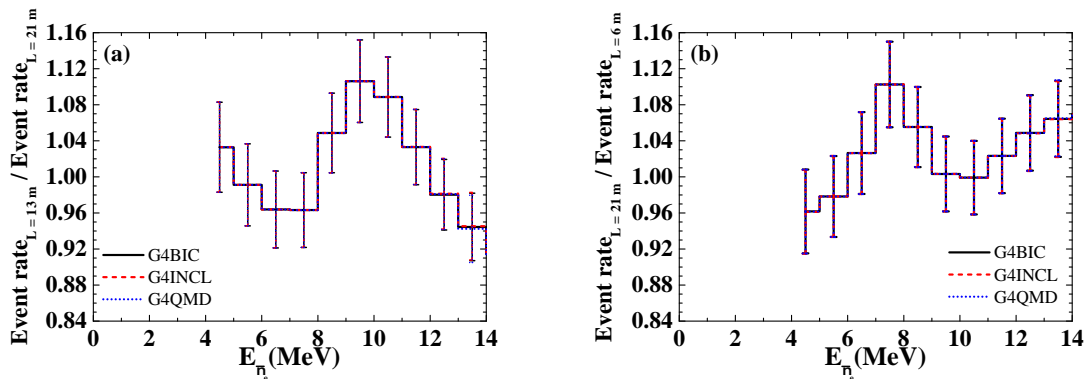


Figure 8. (Color online) Ratios of  $R_{3+1}$ -to- $R_3$  with respect to  $E_{\bar{\nu}_e}$  at different L are shown.

## 5 Summary and Conclusion

In this work, to investigate the existence of sterile neutrino, we propose an electron antineutrino source using  $^{13}\text{C}$  beams based IsoDAR concept for short-baseline electron antineutrino disappearance study. The neutrino source is obtained through  $\beta^-$  decays of unstable isotopes which are generated from the  $^{13}\text{C} + ^9\text{Be}$  reaction. Main isotopes for neutrino production are  $^8\text{Li}$ ,  $^9\text{Li}$ ,  $^{12}\text{Be}$ ,  $^{12}\text{B}$ , and  $^{13}\text{B}$ . They have similar half-lives and reaction Q values of  $\beta^-$  decay, and thus the neutrino energy spectrum with a single broad peak is expected.

The production yields of those isotopes are calculated using three different nucleus-nucleus (AA) reaction models. Even though different yields of the isotopes are obtained from the models, the neutrino spectra are almost identical. This unique feature gives a realistic chance to neutrino oscillation study through shape analysis, regardless of the theoretical AA models considered.

$R_{3+1}$ -to- $R_3$  ratios at  $L = 6$  m and  $L = 13$  m show distinguishable features of the event rates, and thus it can also give a meaningful signal for the existence of the hypothetical  $\nu_s$ . Also, complementary comparison studies among different distance L become feasible. The expected deviation between the maximum and the minimum values is approximately 17%, and thus it can give an effective answer of whether  $P_{3+1}$  models is the most appropriate model for the sterile neutrino.

## Acknowledgments

The work of J. W. Shin is supported by the National Research Foundation of Korea (Grant No. NRF-2015R1C1A1A01054083), the work of M.-K. Cheoun is supported by the National Research Foundation of Korea (Grant No. NRF-2014R1A2A2A05003548 and NRF-2015K2A9A1A06046598).

## References

- [1] LSND collaboration, A. Aguilar-Arevalo et al., *Evidence for neutrino oscillations from the observation of  $\bar{\nu}_e$  appearance in a  $\bar{\nu}_\mu$  beam*, *Phys. Rev. D* **64** (2001) 112007, [[hep-ex/0104049](#)].

- [2] MINIBOONE collaboration, A. Aguilar-Arevalo et al., *Event excess in the MiniBooNE search for  $\bar{\nu}_\mu \rightarrow \bar{\nu}_e$  oscillations*, *Phys. Rev. Lett.* **105** (2010) 181801, [[1007.1150](#)].
- [3] G. Mention, M. Fechner, T. Lasserre, T. A. Mueller, D. Lhuillier, M. Cribier et al., *Reactor antineutrino anomaly*, *Phys. Rev. D* **83** (2011) 073006, [[1101.2755](#)].
- [4] C. Giunti and M. Laveder, *Statistical significance of the gallium anomaly*, *Phys. Rev. C* **83** (2011) 065504, [[1006.3244](#)].
- [5] A. B. Balantekin, *Reactor antineutrinos and nuclear physics*, *Eur. Phys. J. A* **52** (2016) 341.
- [6] ICECUBE collaboration, M. G. Aartsen et al., *Searches for Sterile Neutrinos with the IceCube Detector*, *Phys. Rev. Lett.* **117** (2016) 071801, [[1605.01990](#)].
- [7] M. Cribier et al., *Proposed Search for a Fourth Neutrino with a PBq Antineutrino Source*, *Phys. Rev. Lett.* **107** (2011) 201801, [[1107.2335](#)].
- [8] A. Gando and others, *CeLAND: search for a 4th light neutrino state with a 3 PBq  $^{144}\text{Ce}$ - $^{144}\text{Pr}$  electron antineutrino generator in KamLAND*, [1312.0896v2](#).
- [9] G. Bellini et al., *SOX: Short distance neutrino Oscillations with BoreXino*, *JHEP* **2013** (2013) 38, [[1304.7721](#)].
- [10] A. Bungau, A. Adelmann, J. R. Alonso, W. Barletta, R. Barlow, L. Bartoszek et al., *Proposal for an Electron Antineutrino Disappearance Search Using High-Rate  $^8\text{Li}$  Production and Decay*, *Phys. Rev. Lett.* **109** (2012) 141802, [[1205.4419](#)].
- [11] N. E. Davison, M. J. Canty, D. A. Dohan and A. McDonald,  *$^9\text{Be}(p,2n)^8\text{B}$  reaction as a neutrino source*, *Phys. Rev. C* **10** (1974) 50–53.
- [12] L. A. Mikaelian, P. E. Spivak and V. G. Tsinoev, *A proposal for experiments in low-energy antineutrino physics*, *Nucl. Phys.* **70** (1965) 574–576.
- [13] DAYA BAY collaboration, F. P. An et al., *Measurement of the Reactor Antineutrino Flux and Spectrum at Daya Bay*, *Phys. Rev. Lett.* **116** (2016) 061801, [[1508.04233](#)].
- [14] Y. Abe et al., *Improved measurements of the neutrino mixing angle  $\theta_{13}$  with the Double Chooz detector*, *JHEP* **2014** (2014) 086, [[1406.7763](#)].
- [15] S.-B. Kim, *Observation of Reactor Electron Antineutrino Disappearance at RENO*, *Nucl. Phys. B Proc. Suppl.* **235–236** (2013) 24–29.
- [16] S.-H. Seo, *New Results from RENO and The 5 MeV Excess*, *AIP Conf. Proc.* **1666** (2015) 080002.
- [17] The DOE/NSF Nuclear Science Advisory Committee, *Opportunities in Nuclear Science—A Long-Range Plan for the Next Decade*, April, 2002, [http://science.energy.gov/~media/np/nsac/pdf/docs/lrp\\_5547\\_final.pdf](http://science.energy.gov/~media/np/nsac/pdf/docs/lrp_5547_final.pdf).
- [18] OECD, *Report of the Working Group on Nuclear Physics*, May, 2008, <http://www.oecd.org/sti/sci-tech/40638321.pdf>.
- [19] The European Science Foundation, *NuPECC Long Range Plan 2010: Perspectives of Nuclear Physics in Europe*, November, 2010, [http://www.nupecc.org/pub/lrp10/lrp2010\\_final\\_hires.pdf](http://www.nupecc.org/pub/lrp10/lrp2010_final_hires.pdf).
- [20] D. F. Geesaman, C. K. Gelbke, R. V. F. Janssens and B. M. Sherrill, *PHYSICS OF A RARE ISOTOPE ACCELERATOR*, *Annu. Rev. Nucl. Part. Sci.* **56** (2006) 53–92.
- [21] I. Alekseev et al., *DANSS: Detector of the reactor AntiNeutrino based on Solid Scintillator*, *JINST* **11** (2016) P11011, [[1606.02896](#)].
- [22] A. P. Serebrov et al., *Neutrino-4 experiment on search for sterile neutrino with multi-section model of detector*, [1605.05909](#).

- [23] G. Boireau et al., *Online monitoring of the Osiris reactor with the Nucifer neutrino detector*, *Phys. Rev. D* **93** (2016) 112006, [[1509.05610](#)].
- [24] Y. Kuroda, S. Oguri, Y. Kato, R. Nakata, Y. Inoue, C. Ito et al., *A mobile antineutrino detector with plastic scintillators*, *Nucl. Instrum. Meth. A* **690** (2012) 41–47, [[1206.6566](#)].
- [25] J. Ashenfelter et al., *The PROSPECT physics program*, *J. Phys. G* **43** (2016) 113001, [[1512.02202](#)].
- [26] K. N. Abazajian et al., *Light Sterile Neutrinos: A White Paper*, [1204.5379](#).
- [27] S. Agostinelli et al., *GEANT4—a simulation toolkit*, *Nucl. Instrum. Meth. A* **506** (2003) 250–303.
- [28] J. Allison et al., *Geant4 developments and applications*, *IEEE Trans. Nucl. Sci.* **53** (2006) 270–278.
- [29] A. Strumia and F. Vissani, *Precise quasielastic neutrino/nucleon cross-section*, *Phys. Lett. B* **564** (2003) 42–54, [[astro-ph/0302055](#)].
- [30] R. J. Glauber, *Cross-sections in deuterium at high-energies*, *Phys. Rev.* **100** (1955) 242–248.
- [31] R. J. Glauber and G. Matthiae, *High-energy scattering of protons by nuclei*, *Nucl. Phys. B* **21** (1970) 135–157.
- [32] V. N. Gribov, *A reggeon diagram technique*, *Sov. Phys. JETP* **26** (1968) 414–423.
- [33] B. Z. Kopeliovich, *Transparent nuclei and deuteron-gold collisions at relativistic energies*, *Phys. Rev. C* **68** (2003) 044906, [[nucl-th/0306044v4](#)].
- [34] J. F. Ziegler, J. P. Biersack and U. Littmark, *The Stopping and Ranges of Ions in Solids. Vol.1*, 1985.
- [35] *Stopping of Ions Heavier Than Helium*, 2005. [10.1093/jicru/ndi002](#).
- [36] G. Folger, V. N. Ivanchenko and J. P. Wellisch, *The Binary Cascade*, *Eur. Phys. J. A* **21** (2004) 407–417.
- [37] T. Koi, G. Folger, B. Trieu, J. P. Wellisch, I. Corneliu and P. Truscott, *Ion Transport Simulation Using Geant4 Hadronic Physics, Monte Carlo 2005 Topical Meeting ISBN:0-89448-695-0 Chattanooga, Tennessee, April 17-21, 2005*.
- [38] T. Koi et al., *New native QMD code in Geant4, The Joint International Conference on the 7th Supercomputing in Nuclear Applications and the 3rd Monte Carlo 2010 (SNA+MC2010)*, October 17-21, 2010.
- [39] A. Boudard, J. Cugnon, J.-C. David, S. Leray and D. Mancusi, *New potentialities of the Liège intranuclear cascade model for reactions induced by nucleons and light charged particles*, *Phys. Rev. C* **87** (2013) 014606, [[1210.3498v1](#)].
- [40] D. Mancusi, A. Boudard, J. Cugnon, J.-C. David, P. Kaitaniemi and S. Leray, *Extension of the Liège intranuclear-cascade model to reactions induced by light nuclei*, *Phys. Rev. C* **90** (2014) 054602, [[1407.7755](#)].
- [41] “GEANT4 Physics Reference Manual, <http://geant4.web.cern.ch/geant4/support/index.shtml>.”
- [42] “GEANT4, <http://geant4.cern.ch/>.”
- [43] K. Niita, S. Chiba, T. Maruyama, H. Takada, T. Fukahori, Y. Nakahara et al., *Analysis of the  $(N, xN')$  reactions by quantum molecular dynamics plus statistical decay model*, *Phys. Rev. C* **52** (1995) 2620–2620, [[nucl-th/9508004](#)].
- [44] S. Furihata, *Statistical analysis of light fragment production from medium energy proton-induced reactions*, *Nucl. Instrum. Meth. B* **171** (2000) 251–258, [[nucl-th/0003036](#)].

- [45] A. Boudard, J. Cugnon, S. Leray and C. Volant, *Intranuclear cascade model for a comprehensive description of spallation reaction data*, *Phys. Rev. C* **66** (2002) 044615.
- [46] P. Truscott, *Treatment of Radioactive Decay in Geant4*, *Tech. Rep. Qinetiq* **60** (2002) 2966–2983.
- [47] S. Hauf, M. Kuster, M. Batič, Z. W. Bell, D. H. H. Hoffmann, P. M. Lang et al., *Radioactive Decays in Geant4*, *IEEE Trans. Nucl. Sci.* **60** (2013) 2966–2983, [[1307.0996](#)].
- [48] *ENSDF*, <http://www.nndc.bnl.gov/ensdf/>.
- [49] A. Strumia and F. Vissani, *Neutrino masses and mixings and ...*, [hep-ph/0606054v3](#).
- [50] M. C. Gonzalez-Garcia, M. Maltoni, J. Salvado and T. Schwetz, *Global fit to three neutrino mixing: critical look at present precision*, *JHEP* **2012** (2012) 123, [[1209.3023](#)].
- [51] G. H. Collin, C. A. Argúelles, J. M. Conrad and M. H. Shaevitz, *First Constraints on the Complete Neutrino Mixing Matrix with a Sterile Neutrino*, *Phys. Rev. Lett.* **117** (2016) 221801, [[1607.00011](#)].